Version of Record: https://www.sciencedirect.com/science/article/pii/S0017931021014459
Manuscript_9974e54939eeab3ac587ac6297535733

Determination of thermal conductivity, thermal diffusivity and specific heat capacity of porous silicon thin films using the 3ω method

Sobhan Erfantalab, Giacinta Parish, Adrian Keating

School of Engineering, The University of Western Australia, 35 Stirling Hwy, Crawley, WA, 6009, Australia

Abstract

Here the thermal transport properties of low thermal conductivity porous silicon thin films attached to high thermal conductivity silicon substrates are studied using the 3ω method implemented over the 100 Hz to 33 kHz frequency range. The thermal conductivity and thermal diffusivity of the films are extracted using temperature impedance monitoring of electrical contacts deposited on films, combined with an extended-frequency, multi-layer thermal model. From the extracted thermal conductivity and diffusivity of the films, the heat capacity could be determined. Validation of the approach is performed using the known properties of thick substrate glass and SU-8 layers spun on silicon substrates, the latter ranging in thickness from 1.35 to 12.5 µm. The technique was then applied to porous silicon films with porosities ranging from 45% to 77%. The extracted thermal properties for as-fabricated films show a reduction of thermal conductivity and diffusivity from 1.7 to 0.15 W/mK and 1.9 to 0.2 mm^2/s, respectively as the porosity increases. After passivation by annealing in nitrogen and at 600°C, the same films exhibited higher values of thermal conductivity and diffusivity ranging from 2.7 to 0.7 W/mK and 2.5 to 0.65 mm^2/s. The ability to extract both thermal conductivity and thermal diffusivity for these films removes the need to make assumptions around specific heat capacity, commonly made during analysis of porous media. These results show for the first time a monotonic increase in specific heat capacity of porous silicon films as a function of porosity.

Keywords:

3ω method, porous silicon, thin film, thermal conductivity, thermal diffusivity, specific heat capacity, SU-8

Introduction

Porous silicon (PS), formed by electrochemical anodisation of crystalline silicon, has gained a lot of interest due to the ability to tailor its optical, electrical and thermal properties through easily controllable porosity [1, 2]. This ability, combined with the high surface to volume ratio, enables PS to constitute a low-cost platform to achieve fabrication of highly sensitive sensors [3]. A potential new application for PS is in thermal sensors [4, 5], for which dynamic performance demands thorough knowledge of the thermal properties (thermal conductivity and heat capacity) of the material in order to accurately control the thermal time constant. The low thermal conductivity of PS, several orders of magnitude lower than silicon, was first identified by Lang et al. [6]. The presence of nanopores with an average crystallite size less than the mean

free path of phonons in silicon (Λ_{si} ~ 43 nm [7]) has been identified to be a strong factor in this low thermal conductivity [8]. Since then, various studies have focused on measuring and understanding the thermal conductivity of PS in order to use this knowledge to achieve high thermal isolation within a silicon based platform [9, 10]. However, the specific heat capacity of PS has not been well studied and it is often assumed to be constant (independent of porosity) and equal to the specific heat capacity of bulk silicon. The film porosity appears only in the calculation of heat capacity by scaling the specific heat capacity of bulk silicon by the lower density of PS [11]. The bulk value of specific heat capacity is commonly measured using methods such as scanning differential calorimetry [12], however such methods may not be easily applied to novel materials such as nanostructured [13] and porous materials [14] for which a bulk structure is hard to form. In some cases where specific heat capacity is not known it is reasonable to assume the same bulk values as for another similarly dense material, such as silicon and silicon dioxide, however, for many nanostructured or porous materials in which density and/or surface to volume ratio is significantly different, such an approximation is not necessarily valid. This means that direct measurement is preferable however in the case of porous silicon, fabricating suitable test structures to measure the properties of the films is challenging, as the films are highly reactive and unstable [15]. In some cases, porous silicon can only be studied by sintering the films to very high temperatures, providing some degree of stability but affecting the pore morphology [16] and, more importantly, the thermal parameters.

Different methods used in the literature for characterising thermal properties of thin films and especially PS can be summarised broadly as contact and non-contact methods. In non-contact methods including photoacoustic spectroscopy [17], laser pump-probe [18], lock-in thermography [16] and scanning micro-Raman spectroscopy [19], the material under study is locally illuminated and the respective temperature variation is monitored to investigate the thermal properties. However, because of wavelength and porosity dependent optical absorption and scattering of the light, the input power applied to the sample under test has a large uncertainty, preventing direct thermal conductivity determination. Nevertheless, these methods can be used to determine the thermal diffusivity of the material by measuring the dynamic temperature variation where the thermal data depends on the optical modulation frequency which can be accurately controlled and known. This measurement of thermal diffusivity can be used to extract the thermal conductivity but requires knowledge or assumptions about the specific heat capacity. To extend the capability of non-contact thermal measurement, a recent study compared the photoacoustic response amplitude in the presence and absence of water to estimate the thermal conductivity of PS films [20]. However, control over the ability to uniformly fill all the nano-scale sized pores with water (thermal conductivity = 0.6 W/mK [21]) can compromise the accuracy of those measurements. By comparison, contact methods usually deposit micro-scale conductive features onto thin films, enabling approaches including the 3ω method [22], transient thermo-reflectance [23] or surface probing using scanning thermal microscopy [24]. These methods utilise delivery of a known quantity of heat, concentrated in a micro-structure in intimate contact with the film, so that subsequent measurement of the temperature allows accurate extraction of the thermal conductivity. Furthermore, expanding the capabilities of a contact method to allow simultaneous measurement of thermal conductivity and diffusivity would facilitate studying the heat capacity for the structure under study.

The 3ω method, originally presented by Cahil [25], is perhaps the most widely used and accurate technique to study the thermal properties of different materials [26-28]. This method is usually implemented with a linear approximation known as the "slope method" for thermal conductivity estimation of the bulk and thick film materials [26]. Extension of the slope method to thin, low thermal conductivity films on a highly conducting substrate, which is typical of highly porous films, requires high resolution lithography to confine the thermal penetration depth, only achievable using e-beam writing techniques [29]. Moreover, the majority of previous reports using the 3ω method for thin films were based on utilizing a simple thin film on substrate thermal resistance model, which operates at low frequencies (<1 kHz) to avoid any complex interactions between the film and substrate [27, 30]. Thermal characterisation beyond 1 kHz requires a more complex model as well as careful attention to other sources of third harmonic distortion that could lead to inaccuracy of the 3ω measurement. Tong et al. [31] and Borca-Tasciuc et al. [32] have considered models that avoid the use of the slope method, but measurements into the high frequency range to confirm these models are lacking. Raudzis et al. [33] has also investigated high frequency extension of the 3ω measurement but only used the in-phase part of the response so that the measurement failed to robustly determine the thermal parameters. Olson et al. [34] showed that the 3ω method can be used for extracting the thermal conductivity and heat capacity of SiO_2 films on silicon, however, the measurement was limited to a maximum of 8 kHz, which did not capture important high frequency variations that occur in thin film on substrate multilayer structures.

In this paper, the 3ω method is used to study the thermal properties of thin, low thermal conductivity PS films. A multilayer thermal model [32] is utilized to avoid the limitations of the linearisation or thermal resistance approximation in the 3ω method. The theoretical models [31, 32], predict a roll-off and dip in in-phase and out-of-phase parts of the response which are directly related to the thickness and thermal diffusivity of the film. The experiments showed that increasing the measurement frequency up to 33 kHz can reveal these important features, which also enhances the robustness of the model fittings for thermal studies. The measurements were validated using different materials ranging from bulk glass to different thicknesses of SU-8 thin films on silicon, verifying the accuracy of the method for thin film thermal analysis. Importantly, the validation showed that such films can be thin (in this case 1.35 -12.5 μm) and can remain attached to the high conductivity substrate (in this case silicon). Next, an analysis of SU-8 film thickness and thermal data extraction is presented to find a lower limit for thin film thickness for accurate thermal data extraction. Finally, this method was applied to achieve accurate, simultaneous determination of thermal conductivity and thermal diffusivity of PS films, with those extracted properties then used to determine the specific heat capacity as a function of porosity. The results show for the first time that the specific heat capacity of PS films increases with increasing porosity, calling into question the assumption of a constant specific heat capacity used in many previous reports [9, 18, 35-38]. One additional aspect of investigation in this work is that the PS films were measured in the as-fabricated as well as passivated form, with passivation undertaken by rapid thermal annealing at low temperature (600 °C) in nitrogen. Passivation of these films is an important process which allows robust photolithographic techniques to be used [39, 40] to form micro- and opto-electronic devices, and also stabilises the physical properties [41, 42]. The passivation conditions used for this work are such that films do not become sintered, so that the pores remain open.

Experimental details

Porous silicon fabrication: Porous silicon samples were fabricated by electrochemical anodisation of moderately doped silicon (100) wafers with a nominal resistivity of 0.08 – 0.12 Ω-cm and thickness of 270 ± 30 µm. The wafers were cleaned by dipping into a 49 wt% HF and ethanol solution (volume ratio 1:4). The anodisation took place in a 49 wt% HF and ethanol solution (volume ratio 1:1) using constant current in the dark and at room temperature. The porosity of the films was controlled via the current density while the respective thickness of each sample was controlled by the anodisation time. Constant current of 5, 8, 10 and 130 mA/cm^2 was used to achieve samples with porosities of 45%, 55%, 66% and 77% and thicknesses of 5, 5.3, 6.1 and 3 µm, respectively. The fabricated PS films were then annealed at 600 °C for 6 minutes under nitrogen flow at 1000 sccm [42]. The porosity of the films was extracted from fitting of the optical reflectance measured between 400 – 1000 nm while the thickness was determined by scanning electron microscopy (SEM) cross section imaging.

SU-8: SU-8 2010 (Kayaku [43], 58% solid) photoresist was diluted using cyclopentanone thinner to achieve SU-8 thin films with varying thicknesses. The photoresist was spun onto the same blank silicon substrates as used for PS fabrication. Prior to deposition, the substrate was solvent- and then HF-cleaned and finally dehydrated at 110 °C for 5 minutes, to increase the deposition uniformity and adhesion of the films to the silicon substrate. The SU-8 films were then soft baked (at 95 °C), exposed to ultraviolet light, hard baked (at 95 °C) and finally rinsed in deionised water. The final thickness of each sample was measured using SEM cross-section imaging.

Glass sample: Low iron soda-lime float-glass (Knittel glass, Germany) with approximate thickness of 1 mm, commonly used for microscope slides, was solvent cleaned and used.

Sample preparation for 3ω method: Standard photolithographic and thermal evaporation processes were carried out in a class 1000 cleanroom to define the metallic pattern of the resistive devices required for the 3ω experiment. A schematic of the device is illustrated in Figure 1 and consists of a line heater of length l = 2.5 mm and width of $2b$ = (28.5 ± 0.2) µm. Also, to define heater lines on as-fabricated PS samples, for which photolithographic methods cannot be used, a thin (thickness ~ 80 µm) stencil shadow mask was used. The features created using the shadow mask have the same length but were typically wider, with a width of $2b$ = (45 ± 2) µm. In all cases gold was used for the metallisation and was deposited at a rate of 2 nm/second using thermal evaporator to the final thickness of 150 nm. A thin layer (10 nm) of chromium was deposited below the gold to increase the adhesion between gold and the film. A standard acetone lift-off process was used for the samples that had undergone a photolithographic patterning process. The metal contact pads (1 mm × 1 mm) were wire-bonded using a small amount of conductive epoxy (MG chemicals, 8330S) which has been demonstrated to give reliable electrical connection to PS films, causing no damage to the fragile PS structure [40]. Finally, the wires were soldered to an external printed circuit board (PCB) for the subsequent measurements. The heaters thus formed had a typical resistance of 30 Ω and 18 Ω for 28.5 µm and 45 µm heater widths, respectively. As the temperature coefficient of resistance (TCR) is a key parameter required in the 3ω method [26], measurements in the range of (25 – 60) °C were performed. A platinum resistance temperature detector (PT1000) with a 2 mm probe diameter was also bonded using conductive epoxy at a close distance (< 1 cm) to the deposited metallic heater, to monitor the temperature of the structure. The PCB was then slowly heated with temperature steps of 2 °C using a hotplate, and the resistance of the metallic

heater was recorded after 30 seconds of stabilisation time. The TCR of the metallic heater was calculated by finding the slope of resistance change with respect to the absolute temperature. An extracted value of TCR = (0.0022 ± 0.0001) K^{-1} was found across all samples, within the range of previously reported values [44].

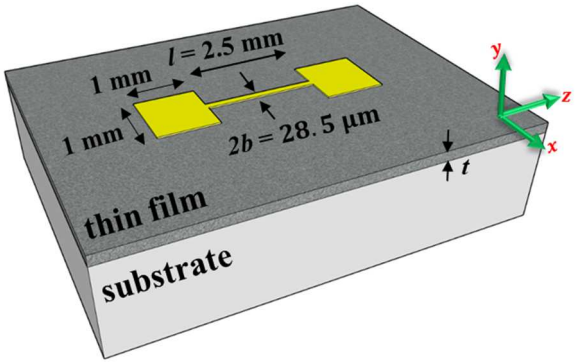

Figure 1: Schematic of gold micro heater/sensor design with deposited metal of length (l = 2.5 mm), width ($2b$ = 28.5 µm or $2b$ = 45 µm) and thickness (t = 150 nm) used for 3ω measurement of thermal properties of the underlying thin film attached to a conducting substrate (SU-8 and PS on Si) or of the substrate only (glass).

Methods

Setup details

The 3ω method used throughout this paper consisted of thermal impedance monitoring of a single/multilayer system exposed to a line heat flux [45]. A sinusoidal voltage at frequency ω (ranging from 100 Hz to 33 kHz) generated by an Agilent 33220A waveform generator (with harmonic distortion < -60 dBc) leads to a Joule heating in the metal heater at the frequency of 2ω. This heat flux results in a variation of the temperature of the heater at the same frequency which consequently will induce an oscillation in the resistance of the heater at the same frequency of 2ω. This resistance oscillation introduces a small variation of voltage at the frequency of 3ω which is proportional to the temperature oscillations across the heater. Monitoring this third harmonic voltage allows the thermal impedance of the structure to be studied.

The schematic of the setup used for the 3ω measurement is presented in Figure 2. Here, to improve the sensitivity to the small voltage variation of the 3ω harmonic, a differential bridge and a variable resistor set to the same resistance as the heater have been used to eliminate the fundamental component and any residual distortion in the input voltage from the final output. The differential stage allows the use of high input power to achieve better signal to noise ratio, without the first harmonic overloading the input to the lock-in amplifier. The variable resistor used was a 2 W Vishay wire wound potentiometer which has a heat sink to reduce heating drift, resulting in a negligible TCR from this resistor across the working frequency range. The differential bridge was made from four OPA2228 operational amplifiers (Texas Instruments) chosen for their small total harmonic distortion (< 0.002%) across the working frequency range. The entire circuit was built into a printed circuit board and enclosed in a metal shield enclosure, enabling low noise and low distortion performance over the entire frequency range. The final output was then input to a SR830 phase sensitive lock-in amplifier. Logarithmic steps were used for the applied frequency, to ensure even sampling of the data on a semi-log-scale, which is important for data fitting and parameter extraction across the entire frequency range. At each

frequency, the time-constant (averaging) for the lock-in was set to 1 second ensuring at least 100 full cycle averages at 100 Hz, and more at higher frequencies. The gain and phase of the amplifier-chain was characterised using a high wattage reference resistor (22 Ω) in place of the sample while grounding both inputs of amplifier U2. By changing the frequency of the input calibration voltage ($V_{i,cal}$) between 300 Hz to 99 kHz, the amplifier-chain can be characterised by reading the output calibration voltage ($V_{o,cal}$) over the same frequencies as the actual 3ω thermal data are determined. The complex gain (G_ω) was subsequently calculated and used to divide out any influence of the circuit to the measured signal, resulting in a high-quality measurement of the device under test (DUT).

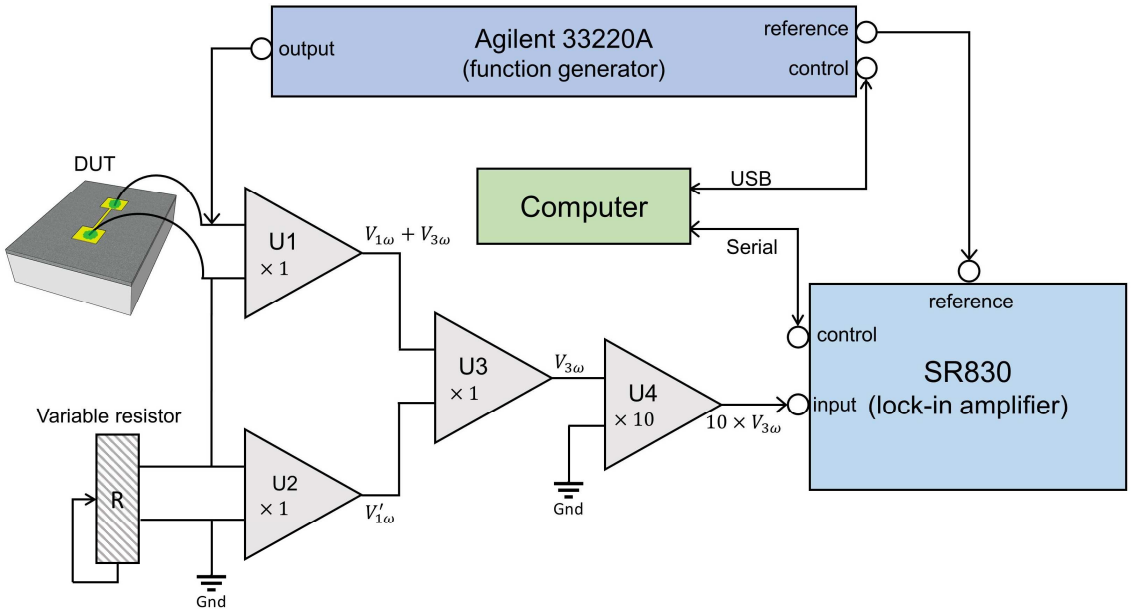

Figure 2 Simplified schematic diagram of the experimental setup used for 3ω measurement. The variable resistor has negligible TCR and is set to the same resistance as heater providing a reference 1st harmonic voltage copy ($V'_{1\omega}$). The first two stages of operational amplifiers form a low noise differential circuit to eliminate the unwanted 1st harmonic voltage ($V_{1\omega}$) from the DUT signal. The final voltage ($V_{3\omega}$) is first amplified to improve the signal to noise ratio before being connected to the lock-in amplifier where the 3rd harmonic is detected using the reference frequency provided by function generator.

All the 3ω measurements were conducted under vacuum (< 10^{-6} Torr). It should be noted that the effect of conducting the experiments under vacuum was more pronounced when the thermal conductivity of the material under study was relatively low (< 1 W/mK) and resulted in thermal conductivity being nominally 5% higher than when the same measurements were conducted in air, for both porous and non-porous materials.

*A*nalytic model

The complex temperature rise of the heater can be estimated using [26]:

$$|\Delta T_{AC}| = \frac{2 \times V_{3\omega}}{V_{1\omega} \times \beta \times G_{3\omega}} \quad (1)$$

where $V_{3\omega}$ is the recorded third harmonic voltage, $V_{1\omega}$ is the applied first harmonic stimulation voltage to DUT, and β is the TCR of the deposited heater. The term $G_{3\omega}$ contains all the

necessary circuit calibration data (gain and phase) to convert the recorded 3rd harmonic voltage into the 3rd harmonic voltage for the DUT. For the general case of a heater deposited on a multilayer films of finite thicknesses, and neglecting the interface thermal resistance between the layers, the temperature change (ΔT_{AC}) across a heater of length *(l)* and width (2*b*), and dissipating power *(P)* can be expressed by the model presented by Borca-Tasciuc [32]:

$$\Delta T_{AC} = \frac{-P}{\pi\, l\, K_{y1}} \int_0^{\infty} \frac{1}{A_1(\lambda)\, B_1(\lambda)} \frac{\sin^2(\lambda b)}{(\lambda b)^2}\, d\lambda \tag{2}$$

where

$$A_{j-1}(\lambda) = \frac{A_j \frac{K_{y,j}\, B_j}{K_{y,j-1}\, B_{j-1}} - \tanh(B_{j-1} t_{j-1})}{1 - A_j \frac{K_{y,j}\, B_j}{K_{y,j-1}\, B_{j-1}} \tanh(B_{j-1} t_{j-1})}, \qquad j = 2 \ldots n, \tag{3}$$

$$B_j = \sqrt{K_{xy,j}\, \lambda^2 + \frac{2i\omega}{D_{y,j}}} \tag{4}$$

$$K_{xy,j} = \frac{K_{x,j}}{K_{y,j}} \tag{5}$$

Here, n is the total number of layers, y is the direction of the thin film growth (cross-plane direction), so that K_x and K_y represent the thermal conductivity in the in-plane and cross-plane directions (also specified in Figure 1), $D_{y,j}$ is the thermal diffusivity of the j'th layer (with j numbered from top to bottom) in the cross plane direction, ω is the angular frequency of the electrical current oscillations and *t* is the thickness of each layer. Moreover, K_{xy} represents the anisotropy in the thermal conductivity for each layer which in this paper is considered equal to 1 (uniform thermal conductivity for all films). Here, the isothermal boundary condition for the bottom of the silicon substrate is reflected in the term given by $A_n = -1/(\tanh(B_n t_n)$ [32]. For data obtained in experiments, the general model given in equations (2-5) was fitted to the in-phase and out-of-phase parts of the response using the nonlinear fitting toolbox library from MATLAB, to extract the thermal conductivity and diffusivity. It should be noted that for the materials used in this paper (SU-8 and PS), due to their relatively low thermal conductivities, the thickness to thermal conductivity ratio is about 5-10 times larger than the typical thin film to silicon interface resistance of 10^{-8} mK/W [46]. This allows the effect of interface resistance to be ignored in the models.

Method validation

To validate the implemented 3ω method, measurements were undertaken using a microscope slide as glass substrate, allowing comparison to that used in similar previous study [34]. A typical experimentally obtained temperature oscillation profile (circles) is shown in Figure 3. Fitting the results (shown with solid lines) with the general model as described above gives values of (1.3 ± 0.05) W/mK and (0.63 ± 0.05) mm^2/s for the thermal conductivity and thermal diffusivity which are within 7% of previous reported values [34]. The uncertainty ranges here, and those following, represent the effect of variation in the input parameters (including heater width, power, TCR and thickness) scaled by the sensitivity to each parameter in the model,

which is estimated to cover 95% probability of variation in the measurement (see supplementary information for details of uncertainty analysis) [47]. The data in Figure 3 illustrates both the importance of low noise operation in a broad frequency range and the power of using a non-linear fitting model. For thick films, the low frequency data can be linearized (on a semi-log-x plot) to extract the thermal conductivity as is typical of the slope method [26]. However, without including high frequencies, the non-linear features of both the in-phase and out-of-phase components are lost, which are critical to achieve simultaneous extraction of both thermal conductivity and diffusivity.

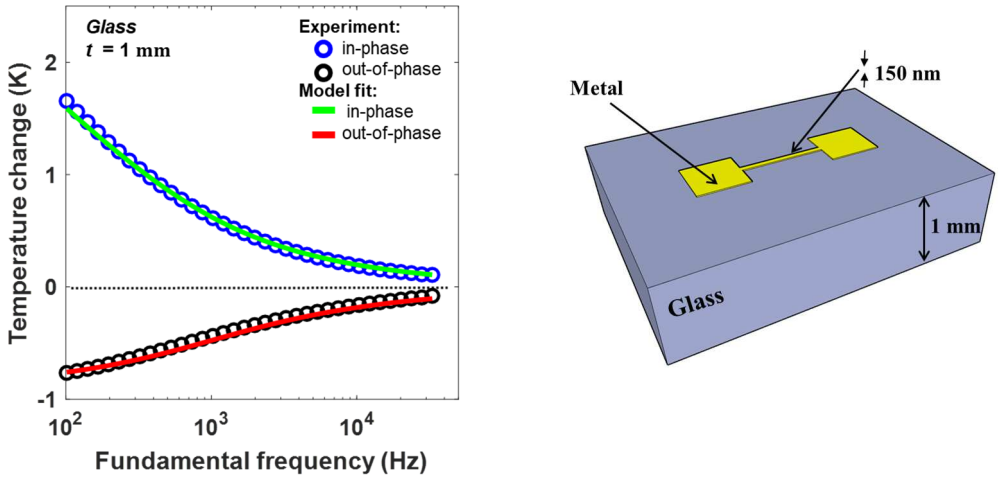

Figure 3 The experimentally recorded temperature oscillation (circles), obtained at 12.5 mW of applied power and model fitting results (solid lines) for 1 mm thick glass substrate as shown schematically on the right-hand side. The RMS error for the line of best fit is less than 50 mK.

Results and discussion

To examine the measurement technique for low thermal conductivity thin films on highly conducting substrates, different thicknesses of SU-8 were spun onto silicon substrates as a test platform. SU-8 polymer was chosen for its deposition simplicity and similar thermal properties to high porosity PS films. Further, they both show a large contrast in their thermal properties in comparison to the high thermal conductivity silicon substrate, an important factor for validating the method for extracting thermal properties for low thermal conductivity thin films on a high thermal conductivity substrate. A typical temperature oscillation obtained for an SU-8 thin film with thickness of 3.15 μm is shown in Figure 4. Here, the frequency of the roll off and dip in the in-phase and out-of-phase parts of the response, is directly related to the thickness and thermal diffusivity (D) of the film, following a frequency dependent thermal penetration depth (λ) according to equation (6) [32]. Most published literature for thin film thermal parameter extraction using the 3ω method has been devoted to only using the in-phase part of the response coupled with the estimated thermal resistance from low frequencies [26, 29], however, including both the in-phase and out-of-phase parts of the response together with a multilayer model that includes the film thickness and substrate contributions to the measurement allows accurate extraction of both the thermal conductivity and thermal diffusivity of the films. In the fitting model used for thin films, the thermal parameters of silicon were independently measured by conducting a separate 3ω measurement on the same silicon wafer used to deposit the films. The extracted thermal parameter values for silicon were (125 ± 5) W/mK and (74 ± 2) mm^2/s for thermal conductivity and diffusivity, respectively.

These values are within 5% of the previously reported values for moderately doped silicon measured using the steady state heating method [48].

$$\lambda = \sqrt{D/2\omega} \tag{6}$$

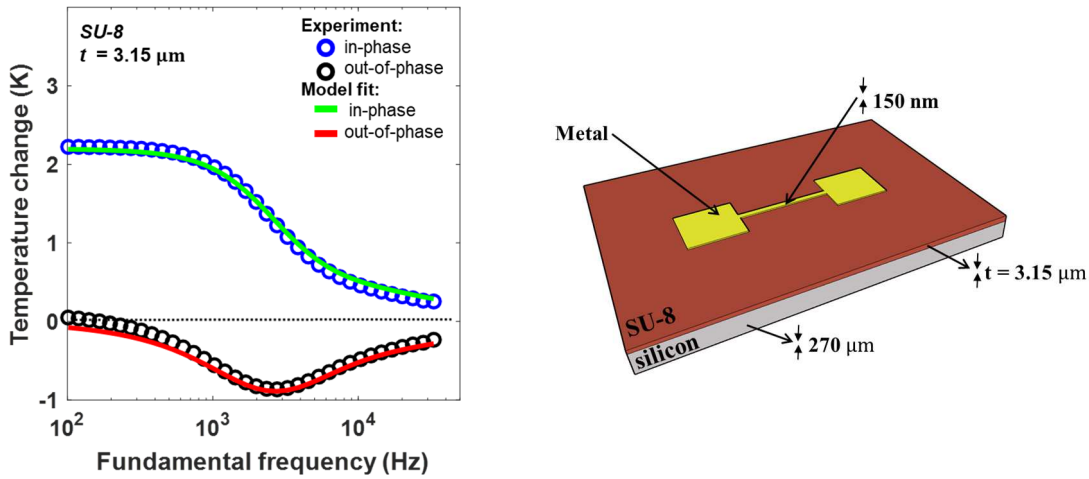

Figure 4 The experimentally recorded temperature oscillation (circles), obtained at 12.5 mW of applied power and model fitting results (solid lines) for 3.15 µm thick SU-8 spun on silicon as shown schematically on the right-hand side. The root mean square (RMS) error for the line of best fit is less than 50 mK.

According to literature [43, 49, 50], SU-8 has a typical thermal conductivity in the range of 0.2 - 0.3 W/mK, depending on deposition conditions. In addition, SU-8 exhibits a density and specific heat capacity of 1200 kg/m^3 and 1.5 kJ/kgK, respectively [50]. Using these values led to an estimated value of thermal diffusivity in the range of 0.11 – 0.16 mm^2/s. The extracted parameters for SU-8 thin films across a range of different thicknesses decreasing from 12.5 µm to 1.35 µm are shown in Figure 5-A. Averaging the values across all thicknesses gives thermal conductivity of 0.24 W/mK and diffusivity of 0.13 mm^2/s, which is within the range of the expected values. From this data, the heat capacity at each thickness was determined and scaled by the density to obtain the specific heat capacity of the SU-8 films (Figure 5-B). The estimated specific heat capacities are within 5% of the published values over all thicknesses except the thinnest sample (1.35 µm), for which the calculated value is 28% higher. This can be explained by the uncertainty in the parameter extraction which is dominated by the thickness uncertainty of ± 50 nm, the effect of which is proportionally highest for thinner films. Also, calculation of thermal penetration depth for SU-8 (equation (6)) shows a minimum of ~1.6 µm at 33 kHz, greater than the thickness of the thinnest SU-8 film in this study (1.35 µm). In the results shown for SU-8 films, thickness of 3.15 µm and above showed consistent thermal fitting results suggesting the minimum thickness to achieve reliable data extraction is at least twice the minimum thermal penetration depth in the experiment. This criterion was applied when choosing the thicknesses of PS films in the remainder of the work. All in all, validation of the method using SU-8 indicates a high accuracy can be expected when applying this measurement system and parameter extraction method to PS films. In addition to the SU-8 validation results, our ability to accurately extract thermal properties from bulk glass and silicon demonstrate the method is extremely robust method across a wide range of thermal properties.

(A)

(B)

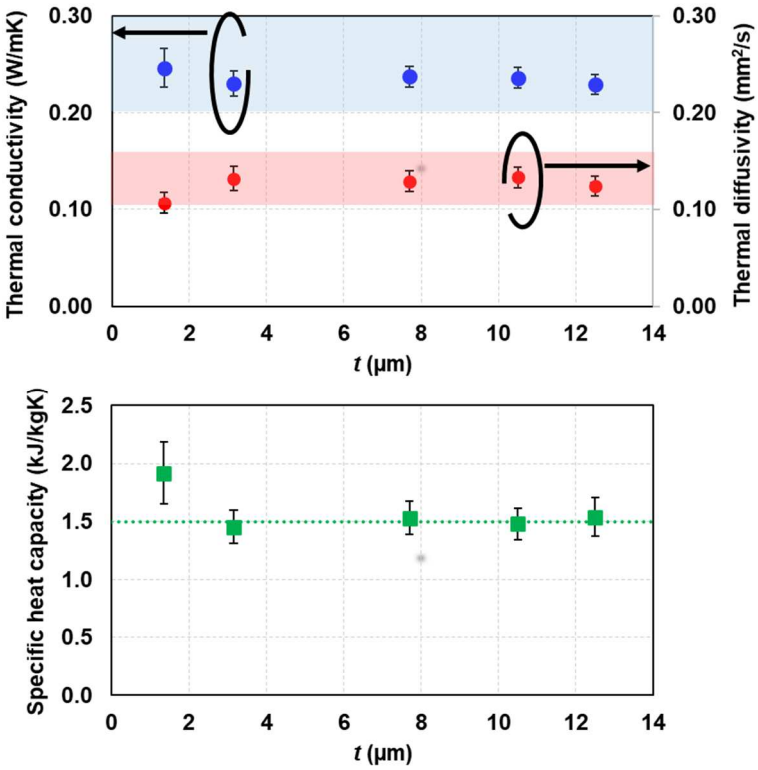

Figure 5 (A) Variation of thermal conductivity (left) and thermal diffusivity (right) extracted from 3ω measurements for SU-8 thin films at different thickness. (B) the calculated specific heat capacity. Previously published literature values [43, 49, 50] are shown as highlighted boxes in (A) for thermal conductivity (blue) and thermal diffusivity (red) and a green dashed line for specific heat capacity in (B).

After validating the measurement method for accurate extraction of both thermal conductivity and diffusivity of thin insulating films on a high conductivity substrate, meso-porous silicon (PS) films were studied. These films were formed on silicon and remained attached to it during the thermal characterisation (Figure 6-A). Most studies attempt to remove the effects of this under layer by detaching the PS films from the substrate or by formation of very thick films, nominally greater than 20-50 µm [16, 18]. However, it is well known that thick porous films can have a significant porosity gradient [51, 52]. Hence thermal measurements of thick films, if associated only with an average porosity, may not be representative of the thermal properties of thin films formed under the same conditions for the same nominal porosity. The approach explored in this work is intended to enable a better understanding of PS thin film properties of lower thicknesses, which also remain attached to the substrate.

The temperature oscillations of the heaters obtained from the 3ω response using equation (1) for passivated PS films at different porosities are shown in Figure 6. While the pore sizes in these films range from 4-70 nm, at the macroscopic scale of the physical measurement (metal feature dimensions) and considering the thermal penetration depth of greater than several hundred nanometres, the film can be considered uniform.

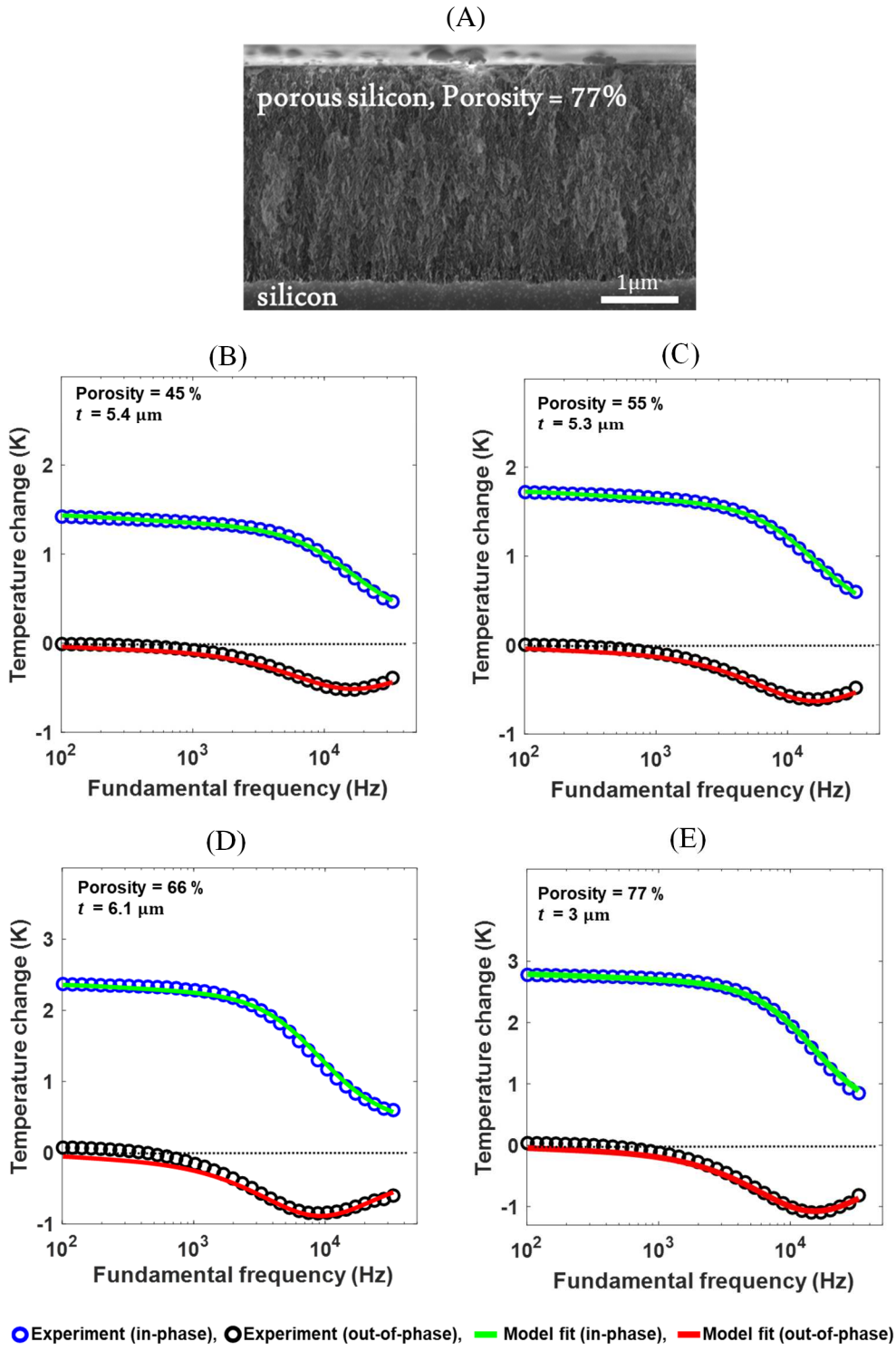

Figure 6 (A) SEM image of the cross-section of a passivated PS film (Porosity = 77%), attached to silicon. (B-E) The experimentally recorded temperature oscillation (circles), obtained at 50 mW of applied power and model fitting results (solid lines) for passivated PS films of different porosities. The root mean square (RMS) error for the line of best fit is less than 50 mK.

The extracted thermal conductivity and diffusivity at the various porosities, for three different positions across each PS sample area of 10 cm^2 are presented in Figure 7. These data provide a measure of the total spatial and numerical uncertainty in the extracted thermal parameters across a sample. The uncertainty in the calculation of thermal conductivity was predominantly sensitive to the uncertainty of the input applied power, TCR, and the thickness of the films. However, the dominant sources of uncertainty for determining the thermal diffusivity were the thickness of the films, fitting error, and film non-uniformity (see supplementary information for details of uncertainty analysis). The thermal conductivity for the passivated PS films shows a decrease from (2.8 ± 0.23) to (0.7 ± 0.05) W/mK while thermal diffusivity decreases from (2.6 ± 0.14) to (0.6 ± 0.07) mm^2/s, resulting from a change in the porosity from 45% to 77%. Extracting both parameters from a single experiment using PS films is unprecedented, as previous reports [9, 17, 18, 53] needed to assume a constant specific heat capacity for the films to extract both parameters.

Following the above experiments, as-fabricated PS films were characterised using micro-heater/sensors formed by direct deposition (no lift-off or processing required) through a shadow mask, with the results also shown in Figure 7. Comparing the two sets of measurements indicates that the passivated films have 2-4 times higher thermal conductivity and thermal diffusivity than the as-fabricated films. However, given that the difference in fabrication processes applied to the two sets of samples included not just passivation but also photolithography, passivated films at two porosities (66% and 77%) were also examined using heaters fabricated by the shadow mask technique for metal patterning. The results for those heaters are highlighted with yellow circles in Figure 7. It can be seen the results for both shadow mask and photolithographic processed heaters show negligible difference. Therefore, the difference in properties for passivated and as-fabricated samples can confidently be attributed to the effects of passivation alone. It should be noted that formation of heaters/sensors having widths tens of microns in size is necessary to generate the heat required for a high signal to noise ratio measurement. However, it was found that the quality and yield of the heaters formed using the shadow mask method was very low compared to photolithography, necessitating careful post examination of the heaters.

(A)

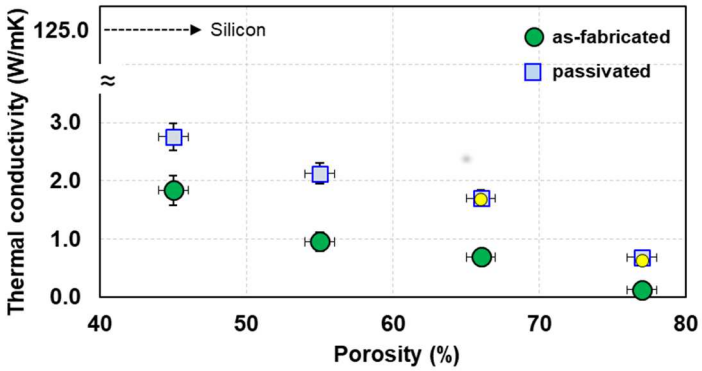

(B)

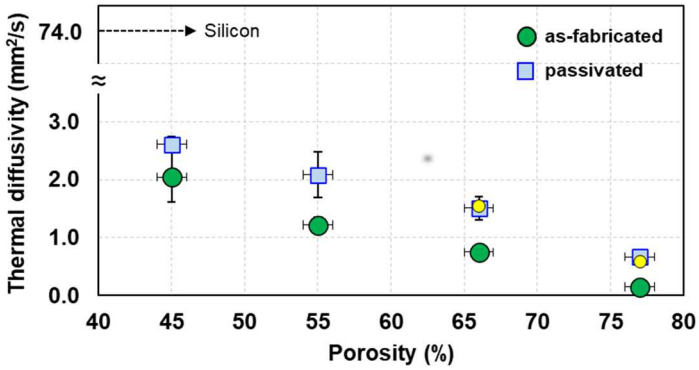

Figure 7 Variation of thermal conductivity (A) and thermal diffusivity (B) extracted from 3ω measurements for passivated and as-fabricated PS films of different porosities; with three measurement points taken for each sample. Yellow circles indicate measurement results for passivated samples with heaters fabricated using the shadow-mask technique (the same as was used for the as-fabricated samples) instead of photolithography.

Simultaneous measurement of both thermal conductivity (K) and diffusivity (D) allows the subsequent calculation of the specific heat capacity (C) for the studied PS films using [21]:

$$\boldsymbol{C = \frac{K}{\rho D}} \qquad (7)$$

where ρ is the density, which for PS films was calculated based on the respective porosity of each sample using $\rho_{ps} = \rho_{si} \times (1\text{-Porosity}/100)$. The variation of calculated specific heat capacity of PS films with porosity is shown in Figure 8 for both as-fabricated and passivated (600°C annealed) samples (see supplementary information for details of uncertainty analysis). For comparison, specific heat capacity of bulk silicon [54] is also indicated. At low porosities, the measured specific heat capacity approaches that expected for bulk silicon (for both as-fabricated and passivated films). As the porosity increases, the specific heat capacity in the PS films gradually increases above that of the starting silicon substrate, up to a factor of 2.1 for as fabricated films of 77% porosity and a factor of 2.9 for passivated films of 77% porosity, the highest porosity studied in this work.

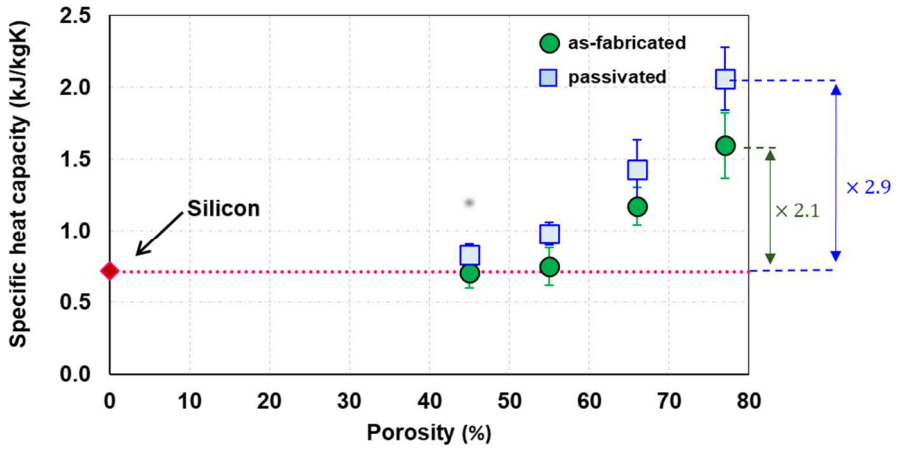

Figure 8 Variation of specific heat capacity with porosity for as-fabricated and passivated PS films, extracted from 3ω measurements. The error bars are calculated using uncertainty in thermal conductivity and diffusivity (as previously defined) and porosity estimation. Dashed red line indicates the literature value for bulk silicon.

The impact of nanopores with average crystallite size less than mean free path of phonons in silicon (Λ_{si} ~ 43 nm [7]) on the thermal conductivity of PS films have been thoroughly discussed in the previous reports [8, 10]. The macroscale considerations assume the specific heat capacity of the porous silicon films is only dependent on the properties of the remaining silicon skeleton, allowing the use of a constant specific heat capacity equivalent to that of silicon. However, this study reveals the importance of the nano-scale open-pore properties on the heat capacity for these porous silicon films and that for high porosities above 50%, such an assumption is invalid. These results are consistent with those that have been reported by Huang et al. for nanoporous Al_2O_3, in which they showed the specific heat capacity is dependent on both the pore size and porosity [14]. Much in the same way that the quantum-confinement effect alters the optical absorption of PS films in the visible range [55], pore sizes comparable to the mean free path of phonons (for silicon Λ_{si} ~ 43 nm [7]) as is the case for films in this work, appear to play a significant role in determining the specific heat capacity of these films. These observations are extremely important if mesoporous films are being considered for use in thermo-resistive sensor applications [4, 5], for which the thermal time constant is a key parameter, determining the fastest video frame rate possible in a thermal imager [56].

Conclusion

The 3ω method was coupled with a multilayer model to enable extraction of thermal properties of low thermal conductivity thin films on highly conducting substrates. The measurements were validated using different thicknesses of SU-8 thin films, demonstrating an accuracy of better than 5%. This approach was then applied to accurately extract the thermal conductivity and diffusivity of porous silicon thin films with thicknesses ranging from 3 to 6 µm over porosity ranges of 45% to 77%, with and without passivation. The specific heat capacity was also extracted and found to increase with porosity, up to a factor of 3 as compared with silicon for the passivated samples of 77% porosity, and doubled for as-fabricated PS films of 77% porosity. This highlights the risk in assuming specific heat capacity in porous silicon is constant

and equal to silicon, an assumption that has been commonly used in many thermal measurement methods.

Acknowledgement

This work was supported by Australian Government Research Training Program Scholarship at The University of Western Australia. The authors acknowledge the support from the Australian Research Council (DP170104266), Western Australian Node of the Australian National Fabrication Facility, and the Office of Science of the WA State Government. The authors acknowledge the facilities, and the scientific and technical assistance of the Australian Microscopy & Microanalysis Research Facility at the Centre for Microscopy, Characterisation & Analysis, and The University of Western Australia, a facility funded by the University, State and Commonwealth Governments.

References

1. Theiß, W., *Optical properties of porous silicon.* Surface Science Reports, 1997. **29**(3-4): p. 91-192.
2. Anderson, R.C., R.S. Muller, and C.W. Tobias, *Investigations of the electrical properties of porous silicon.* Journal of the Electrochemical Society, 1991. **138**(11): p. 3406.
3. Lewis, S.E., et al., *Sensitive, selective, and analytical improvements to a porous silicon gas sensor.* Sensors and Actuators B: Chemical, 2005. **110**(1): p. 54-65.
4. Sharma, P., et al., *Optimising porous silicon electrical properties for thermal sensing applications.* Microporous and Mesoporous Materials, 2020. **312**: p. 110767.
5. Sharma, P., et al., *Engineering 1/f noise in porous silicon thn films for thermal sensing applications.* Microporous and Mesoporous Materials, 2021: p. 111302.
6. Lang, W., et al., *The thermal conductivity of porous silicon.* MRS Online Proceedings Library Archive, 1994. **358**.
7. Chen, G., *Nonlocal and nonequilibrium heat conduction in the vicinity of nanoparticles.* 1996.
8. Gesele, G., et al., *Temperature-dependent thermal conductivity of porous silicon.* Journal of Physics D: Applied Physics, 1997. **30**(21): p. 2911.
9. Amato, G., et al., *Thermal characterisation of porous silicon membranes.* Journal of Porous Materials, 2000. **7**(1-3): p. 183-186.
10. Lysenko, V., et al., *Theoretical and experimental study of heat conduction in as-prepared and oxidized meso-porous silicon.* Microelectronics journal, 1999. **30**(11): p. 1141-1147.
11. Bernini, U., et al., *Determination of thermal diffusivity of suspended porous silicon films by thermal lens technique.* Applied Physics A, 2005. **81**(2): p. 399-404.
12. Hernández‐Sánchez, F., *Heat capacity measurement in polymers using a differential scanning calorimeter: Area measurement method.* Journal of applied polymer science, 2007. **105**(6): p. 3562-3567.
13. Gu, M.X., et al., *Size, temperature, and bond nature dependence of elasticity and its derivatives on extensibility, Debye temperature, and heat capacity of nanostructures.* Physical Review B, 2007. **75**(12): p. 125403.
14. Huang, C.-L., et al., *Specific heat capacity of nanoporous Al2O3.* EPL (Europhysics Letters), 2013. **103**(5): p. 56002.
15. James, T.D., et al., *N2-based thermal passivation of porous silicon to achieve long-term optical stability.* Electrochemical and Solid State Letters, 2010. **13**(12): p. H428.
16. Wolf, A. and R. Brendel, *Thermal conductivity of sintered porous silicon films.* Thin Solid Films, 2006. **513**(1-2): p. 385-390.
17. Bernini, U., et al., *Photo-acoustic characterization of porous silicon samples.* Journal of Optics A: Pure and Applied Optics, 1999. **1**(2): p. 210.

18. Bernini, U., et al., *Evaluation of the thermal conductivity of porous silicon layers by an optical pump-probe method.* Journal of Physics: Condensed Matter, 2001. **13**(5): p. 1141.
19. Lysenko, V., et al., *Thermal conductivity of thick meso-porous silicon layers by micro-Raman scattering.* Journal of Applied Physics, 1999. **86**(12): p. 6841-6846.
20. Dubyk, K., et al., *Thermal properties study of silicon nanostructures by photoacoustic techniques.* Journal of Applied Physics, 2020. **127**(22): p. 225101.
21. Benenson, W., et al., *Handbook of physics*. 2006: Springer Science & Business Media.
22. De Boor, J., et al., *Temperature and structure size dependence of the thermal conductivity of porous silicon.* EPL (Europhysics Letters), 2011. **96**(1): p. 16001.
23. Weisse, J.M., et al., *Thermal conductivity in porous silicon nanowire arrays.* Nanoscale research letters, 2012. **7**(1): p. 554.
24. Gomes, S., et al., *Application of scanning thermal microscopy for thermal conductivity measurements on meso-porous silicon thin films.* Journal of Physics D: Applied Physics, 2007. **40**(21): p. 6677.
25. Cahill, D.G. and R.O. Pohl, *Thermal conductivity of amorphous solids above the plateau.* Physical review B, 1987. **35**(8): p. 4067.
26. Cahill, D.G., *Thermal conductivity measurement from 30 to 750 K: the 3ω method.* Review of scientific instruments, 1990. **61**(2): p. 802-808.
27. Cahill, D.G., M. Katiyar, and J.R. Abelson, *Thermal conductivity of a-Si: H thin films.* Physical review B, 1994. **50**(9): p. 6077.
28. Qiu, L., et al., *In vivo skin thermophysical property testing technology using flexible thermosensor-based 3ω method.* International Journal of Heat and Mass Transfer, 2020. **163**: p. 120550.
29. Moridi, A., et al., *Characterisation of high thermal conductivity thin-film substrate systems and their interface thermal resistance.* Surface and Coatings Technology, 2018. **334**: p. 233-242.
30. Moon, S., et al., *Thermal conductivity of amorphous silicon thin films.* International Journal of Heat and Mass Transfer, 2002. **45**(12): p. 2439-2447.
31. Tong, T. and A. Majumdar, *Reexamining the 3-omega technique for thin film thermal characterization.* Review of Scientific Instruments, 2006. **77**(10): p. 104902.
32. Borca-Tasciuc, T., A. Kumar, and G. Chen, *Data reduction in 3ω method for thin-film thermal conductivity determination.* Review of scientific instruments, 2001. **72**(4): p. 2139-2147.
33. Raudzis, C.E., F. Schatz, and D. Wharam, *Extending the 3ω method for thin-film analysis to high frequencies.* Journal of applied physics, 2003. **93**(10): p. 6050-6055.
34. Olson, B.W., S. Graham, and K. Chen, *A practical extension of the 3 ω method to multilayer structures.* Review of Scientific Instruments, 2005. **76**(5): p. 053901.
35. Benedetto, G., L. Boarino, and R. Spagnolo, *Evaluation of thermal conductivity of porous silicon layers by a photoacoustic method.* Applied Physics A, 1997. **64**(2): p. 155-159.
36. Shen, Q. and T. Toyoda, *Dependence of thermal conductivity of porous silicon on porosity characterized by photoacoustic technique.* Review of scientific instruments, 2003. **74**(1): p. 601-603.
37. Amin-Chalhoub, E., et al., *Thermal conductivity measurement of porous silicon by the pulsed-photothermal method.* Journal of Physics D: Applied Physics, 2011. **44**(35): p. 355401.
38. Lishchuk, P., et al., *Investigation of thermal transport properties of porous silicon by photoacoustic technique.* International Journal of Thermophysics, 2015. **36**(9): p. 2428-2433.
39. Lai, M., et al., *Development of an alkaline-compatible porous-silicon photolithographic process.* Journal of microelectromechanical systems, 2011. **20**(2): p. 418-423.
40. Sun, X., et al., *Enabling high-porosity porous silicon as an electronic material.* Microporous and Mesoporous Materials, 2021. **312**: p. 110808.
41. Lai, M., et al., *Surface morphology control of passivated porous silicon using reactive ion etching.* Journal of microelectromechanical systems, 2012. **21**(3): p. 756-761.

42. James, T., et al., *Low temperature N2-based passivation technique for porous silicon thin films.* Solid state communications, 2009. **149**(33-34): p. 1322-1325.
43. *SU-8 2000.5-2015 Data Sheet*. 2021; Available from: https://kayakuam.com/products/su-8-2000/.
44. Belser, R.B. and W.H. Hicklin, *Temperature coefficients of resistance of metallic films in the temperature range 25 to 600 C.* Journal of Applied Physics, 1959. **30**(3): p. 313-322.
45. Wang, H. and M. Sen, *Analysis of the 3-omega method for thermal conductivity measurement.* International Journal of Heat and Mass Transfer, 2009. **52**(7-8): p. 2102-2109.
46. Wang, H., et al., *Computation of interfacial thermal resistance by phonon diffuse mismatch model.* Materials transactions, 2007. **48**(9): p. 2349-2352.
47. Standardization, I.O.f., *Uncertainty of measurement-Part 3: Guide to the expression of uncertainty in measurement (GUM: 1995)*. 2008: ISO.
48. Asheghi, M., et al., *Thermal conduction in doped single-crystal silicon films.* Journal of applied physics, 2002. **91**(8): p. 5079-5088.
49. Biswas, K.G., et al., *Thermal conductivity of bismuth telluride nanowire array-epoxy composite.* Applied Physics Letters, 2009. **94**(22): p. 223116.
50. Martinez-Duarte, R. and M. Madou, *SU-8 photolithography and its impact on microfluidics.* Microfluidics and nanofluidics handbook, 2011(2006): p. 231-268.
51. Afandi, Y., G. Parish, and A. Keating, *Compensating porosity gradient to produce flat, micromachined porous silicon structures.* Microporous and Mesoporous Materials, 2019. **284**: p. 427-433.
52. Billat, S., et al., *Influence of etch stops on the microstructure of porous silicon layers.* Thin solid films, 1997. **297**(1-2): p. 22-25.
53. Dubyk, K., et al., *Thermal conductivity of silicon nanomaterials measured using the photoacoustic technique in a piezoelectric configuration.* Journal of Physics and Chemistry of Solids, 2019. **126**: p. 267-273.
54. Abe, H., H. Kato, and T. Baba, *Specific heat capacity measurement of single-crystalline silicon as new reference material.* Japanese Journal of Applied Physics, 2011. **50**(11S): p. 11RG01.
55. Kanemitsu, Y., et al., *Microstructure and optical properties of free-standing porous silicon films: Size dependence of absorption spectra in Si nanometer-sized crystallites.* Physical review B, 1993. **48**(4): p. 2827.
56. Niklaus, F., et al., *Performance model for uncooled infrared bolometer arrays and performance predictions of bolometers operating at atmospheric pressure.* Infrared Physics & Technology, 2008. **51**(3): p. 168-177.